Edinburgh, Scotland
EURONOISE 2009
October 26-28

H.J.Rice[1]
C.Clancy[2]
School of Engineering
Trinity College, Dublin, Ireland

Efficient frequency domain calculation of aft fan acoustical modes

ABSTRACT

The use of an efficient wave based discretisation scheme in conjunction with a standard compressible RANS calculation over a shared mesh is presented to model the propagation of aft fan modes in a one tenth scale simulator. The flow regime is split into two potential flow regimes with a shear interface to model the potential jump in the near part of the secondary shear layer. The model runs quickly in a matlab environment on a modest laptop yielding encouraging results.

1.INTRODUCTION

A significant noise component from high by-pass ratio turbofan engines is composed of tonal noise radiated to the rear from the aft fan duct. In order to meet noise reduction goals using emerging technologies in both active and passive control, robust computational tools suitable for use in efficient simulations and "design loops" are necessary. In this paper the suitability of the wave expansion method is investigated as a basis for calculating the propagation of tonal modes in a flow regime generated in a representative design of an engine noise simulator.

In general the flow under consideration will be compressible, rotational and non-homentropic which should require numerical solutions based on the linearized euler equations (LEE). Although commercial implementations of these are now available (eg ACTRAN) many aspects of them are still under development and they are computationally intensive. Closer inspection of the flows under consideration show that rotational aspects are confined chiefly to narrow shear layers and the non-homentropy is confined to regions close to the axis and unlikely to interfere with propagation emanating from the secondary duct. In this spirit Eversman and Okunbor [1] have already proposed the use of a frequency domain finite element propagation model operating in a simplified multi-domain potential flow model with a separate treatment to account for the rotation in the shear layer as a robust computation scheme for this problem. In addition Bailly et al [2] have reported on the study of the comparative performance of Ray theory, potential theory and an LEE calculation of the acoustic field generated by a point source in a sheared flow of profile where it is clear that depending on the position of the source and observer, the simplified models can give quite satisfactory solutions (with minimal computational effort). Caruthers et al [3] have proposed a wave based approach as a highly efficient method in discretising these problems in the frequency domain and have reported on its application to forward fan calculations using a potential formulation. Recently, wave based discretisations of the full LEE are being explored an example of which is the recent paper by Gabard et al [4] where a 2D model has been analysed.

[1]Email address. hrice@tcd.ie
[2]Email address. clancyca@tcd.ie

In this paper the discretisation strategy proposed in [3] will be applied to a multidomain model of the flow from a representation of an engine noise simulator that includes a shear interface between the secondary jet and the outer flow.

2.POTENTIAL FORMULATION

The acoustic field for a high speed irrotational homentropic flow (see for example Howe's [5]) is given by

$$(L(\frac{1}{c_0^2}L) + \frac{1}{\rho_0}\bigtriangledown(\rho_0\bigtriangledown))\psi = 0 \tag{1}$$

Where $\psi(\mathbf{x},\omega)$ is the acoustic velocity potential, the frequency domain operator L is given by

$$L = i\omega + \mathbf{U}_0.\bigtriangledown \tag{2}$$

$\mathbf{U}_0(\mathbf{x})$, $\rho_0(\mathbf{x})$, $c_0(\mathbf{x})$ refer to the background (steady) velocity, density and sonic speed. ω is the circular frequency. The acoustic pressure can be recovered from the potential using

$$p = -\rho_0(i\omega\psi + \mathbf{U}_0.\bigtriangledown\psi) \tag{3}$$

A.Fundamental Axisymmetric Wave Based Solutions

Wave based methods of analysis lead to discretisations using basis functions which are fundamental solutions of the governing system equations. Discretisation strategies may use finite element, volume or difference approaches and result in enhanced wave resolving properties over conventional approaches thus allowing dramatic reductions in nodal density per solution wavelength.

In [3] it has been shown the plane wave solutions propagating in an evenly distributed spread of directions provide a suitable basis set.

The equation 1 admits axisymmetric plane wave solutions for azimuthal mode η of the form

$$\psi(x,r,\phi) = e^{i\eta\phi}e^{-i\lambda_j\mathbf{n}_j.\mathbf{x}(x,r)} \tag{4}$$

where $\mathbf{n}_j$ is a unit vector in the x,r plane. The wave number λ_j is given by

$$\lambda_j^{1,2} = \frac{i\mathbf{B}_0.\mathbf{n}_j \pm \sqrt{4K_0^2(1-(\mathbf{M}_0.\mathbf{n}_j^2)) - (\mathbf{B}_0.\mathbf{n}_j)^2}}{2(1-(\mathbf{M}_0.\mathbf{n}_j)^2)} \tag{5}$$

where

$$\mathbf{B}_0 = 2i\frac{\omega}{c_0}\mathbf{M}_0 + \mathbf{U}_0.\nabla(\frac{1}{c_0^2})\mathbf{U}_0 + \frac{1}{c_0^2}\mathbf{U}_0.\nabla\mathbf{U}_0 - \nabla\ln\rho_0 - \frac{\mathbf{x}}{r} \tag{6}$$

and

$$K_0^2 = (\frac{\omega}{c_0})^2 - i\omega\mathbf{U}_0.\nabla(\frac{1}{c_0^2}) - \frac{\eta^2}{r^2} \tag{7}$$

B.Discretisation strategy

Following the general finite difference strategy in [6], the computational template associated with each node (at position $\mathbf{x}_0$) is given by

$$\psi(\mathbf{x}_0) = \sum_{j=1}^{m} e^{-i\lambda_j(\mathbf{x}_0)}\gamma_j \tag{8}$$

where γ_j are the complex amplitudes of the participating basis functions. In matrix form, equation 8 can be stated as

$$\psi_0 = \mathbf{h}_0\boldsymbol{\gamma} \tag{9}$$

when ψ is evaluated at all the neighbouring nodes in the computational cell centred on $\mathbf{x}_0$, equation 9 can be restated as

$$\boldsymbol{\psi} = \mathbf{H}\boldsymbol{\gamma} \tag{10}$$

Combining equations 9 and 10 then gives the computational template as

$$\psi_0 - \mathbf{h}_0\mathbf{H}^{-1}\boldsymbol{\psi} = 0 \tag{11}$$

$\mathbf{H}^{-1}$ denotes the pseudo inverse of the function matrix $\mathbf{H}$ and the number of basis functions used m in equation 8 must be greater than the number of neighbouring points in the computational cell to ensure consistent interpolation at the nodal points.

B.Boundary conditions

Dirichlet restraints may be indirectly implemented by restraining individual rows of the system matrix.

If a Neumann type restraint is required of the form for example of

$$\frac{\partial\psi(\mathbf{x}_0)}{\partial\mathbf{n}_0} = Q_0 \tag{12}$$

then one approach is to augment the local template equation 10 to

$$\begin{pmatrix} \boldsymbol{\psi} \\ Q_0 \end{pmatrix} = \mathbf{H}_{aug}\boldsymbol{\gamma} \tag{13}$$

where

$$\mathbf{H}_{aug} = \begin{pmatrix} \mathbf{H} \\ \frac{\partial\mathbf{h}_0}{\partial\mathbf{n}_0} \end{pmatrix} \tag{14}$$

Then the template equation 11 can be expressed as

$$\psi_0 - \mathbf{h}_0(\mathbf{H_{aug}})^{-1}_{left}\boldsymbol{\psi} = \mathbf{h}_0(\mathbf{H_{aug}})^{-1}_{right}Q_0 \tag{15}$$

using left and right (single column) partitioning of $(\mathbf{H}_{aug})^{-1}$.

"Natural" radiation conditions can be implemented simply by using half templates on the boundaries and restricting the selection of wavenumbers and direction to those which generate a sector of outward propagating waves.

The implementation of the shear layer interface requires the splitting of the domain into an upper and lower domain where pure potential flow regimes pertain following the general strategy proposed in [1].

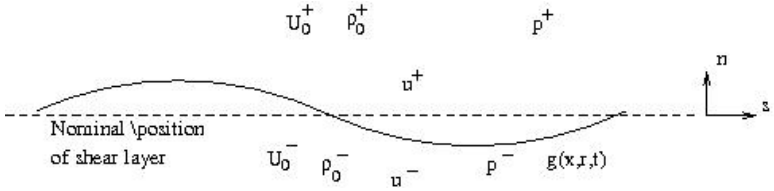

Figure 1: Shear layer model

Entities just above and below the shear layer are denoted by the + and - superscripts and the shear layer is assumed to move with displacement $g(x,r,t)$ about a nominal position which as a first approximation is locally flat. In the discretisation nodes which are on the nominal shear layer are assigned two degrees of freedom ψ^+ and ψ^- and as non overlapping half templates will be formed on the interface, two boundary conditions must then be implemented to make the over all system matrix non-singular.

The kinematic boundary condition may be stated using a mass continuity balance across the layer as

$$\rho_0^+ u_n^+ = \rho_0^+ (i\omega + U_{0s}^+ \frac{\partial}{\partial s})g = \rho_0^- u_n^- = \rho_0^- (i\omega + U_{0s}^- \frac{\partial}{\partial s})g \tag{16}$$

where the motion of the layer is assumed to be small and time harmonic and $u^\pm$ refers to the acoustic velocities above and below the layer. If the surface is flat and the steady components of the flow are assumed to be uniform, we can assert that

$$U_{n0}^\pm = \frac{\partial U_{s0}^\pm}{\partial s} = \frac{\partial U_{s0}^\pm}{\partial n} = 0 \tag{17}$$

This allows us to eliminate the displacement function g from equation 16 and express the kinematic boundary condition as

$$i\omega \frac{\partial \psi^+}{\partial n} + U_{s0}^- \frac{\partial^2 \psi^+}{\partial n \partial s} = i\omega \frac{\partial \psi^-}{\partial n} + U_{s0}^+ \frac{\partial^2 \psi^-}{\partial n \partial s} \tag{18}$$

On the boundary nodes the kinematic condition 18 can be implemented using the template

$$(i\omega \frac{\partial \mathbf{h}_0^+}{\partial n} + f(s) U_{s0}^- \frac{\partial^2 \mathbf{h}_0^+}{\partial n \partial s})(\mathbf{H}^+)^{-1} \boldsymbol{\psi}^+ = (i\omega \frac{\partial \mathbf{h}_0^-}{\partial n} + f(s) U_{s0}^+ \frac{\partial^2 \mathbf{h}_0^-}{\partial n \partial s})(\mathbf{H}^-)^{-1} \boldsymbol{\psi}^- \tag{19}$$

The function $f(s)$ can be used to fade out the "jump" effect in more remote regions of the shear layer to avoid the emergence of non-physical solutions as discussed by the authors [7]. The dynamic boundary condition results from the equality of pressure across the shear layer ...

$$p^+ = p^- \tag{20}$$

which when substituted into the linearised Bernoulli equation subject to the constraints in equation 17 give

$$i\omega\rho_0^+\psi^+ + \rho_0^+ U_{s0}^+ \frac{\partial \psi^+}{\partial s} = i\omega\rho_0^-\psi^- + \rho_0^- U_{s0}^- \frac{\partial \psi^-}{\partial s} \tag{21}$$

The condition 21 can then be implemented using the template

$$i\omega\rho_0^+\psi_0^+ + f(s)\rho_0^+ U_{s0}^+ \frac{\partial \mathbf{h}_0^+}{\partial s}(\mathbf{H}^+)^{1-}\boldsymbol{\psi}^+ = i\omega\rho_0^-\psi_0^- + f(s)\rho_0^- U_{s0}^- \frac{\partial \mathbf{h}_0^-}{\partial s}(\mathbf{H}^-)^{1-}\boldsymbol{\psi}^- \tag{22}$$

3.AFT FAN SIMULATION

The above methodology is now applied to a proposed design of a one tenth scale engine simulator whose (primary) turbine is driven by a cooled nitrogen jet. Of concern here is the emergence of particular acoustic modes from the (secondary) bypass duct at specified blade pass frequencies.

A.Preliminary background flow analysis

A preliminary unstructured irregular mesh containing 9737 nodes and 18821 elements was developed to model the region within 1.5 diameters and about twice the length of the supplied geometry using gambit. The intention was to use the same mesh for the flow and acoustic calculations. Some mesh refinement was done in the regions of the secondary and primary exhausts as shown in figure 5 to account for the locally high flow rates which would require higher mesh densities for satisfactory discretisation. The background flows were calculated using a compressible RANS simulation with zero shear wall conditions and a Spalart Allmaras dissipation model with a Sutherland viscosity model using the commercial code FLUENT and representative duct entry conditions.

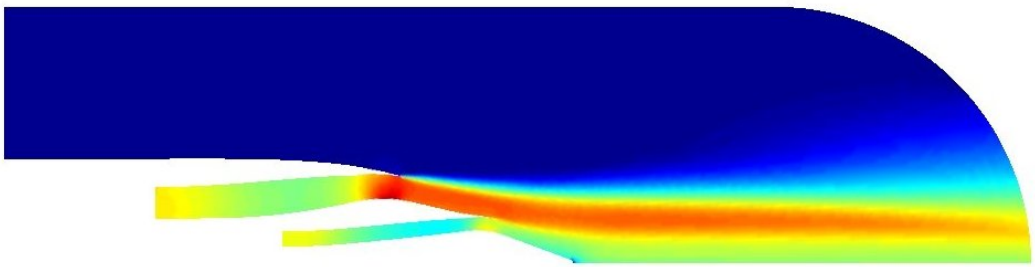

Figure 2: Axial Velocity

The plot of velocity shows a peak speed of about Mach 0.8 in the region of the secondary inlet. This is still subsonic and required the use of significant mesh refinement in this region in order to be able to maintain frequency resolution. The speed in the overall jet is approximately Mach 0.6. Some mesh refinement was used here also. In addition to calculating the background flow parameters, plots on the vorticity and the entropy are included in an attempt to qualitatively assess the assumption of irrotational homentropic flow. The flow is predominantly irrotational except for the area beyond the lip at the secondary exit. The entropy plot shows a homentropic assumption to be reasonable for this calculation as the only region where there is a significant gradient occurs quite close to the axis. This will not be expected participate in acoustic transmission for higher modes emanating from the secondary duct.

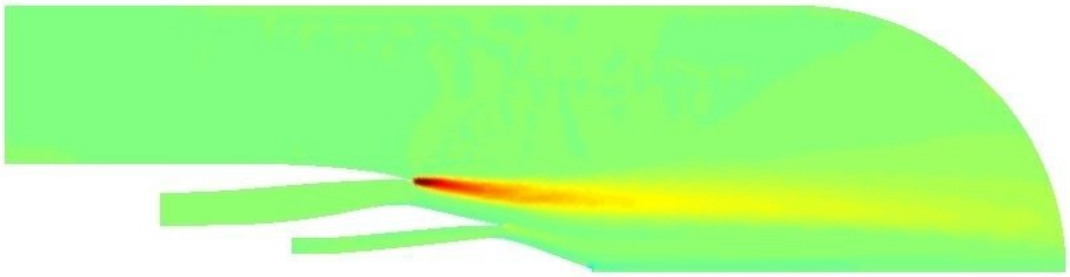

Figure 3: Vorticity

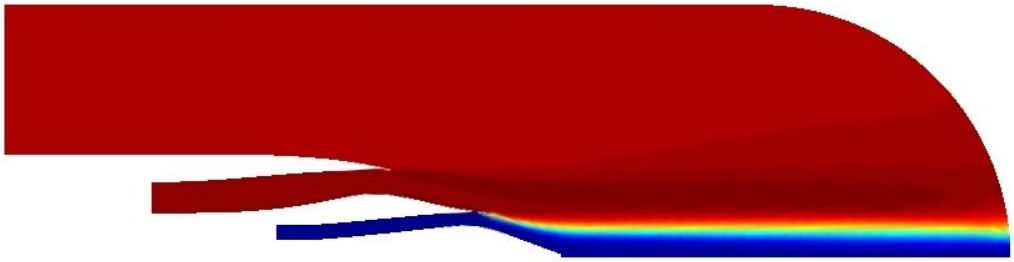

Figure 4: Entropy

A.Refined background flow analysis

The system was now re-meshed with a shear interface boundary (manually) included along the ridge of the secondary vorticity pattern. Nodes on the interface were assigned a second degree of freedom (upper and lower potentials) and together with some other mesh refinement informed by the preliminary calculation, this resulted in a system with 13324 degrees of freedom. The RANS calculation was then re-run with a laminar dissipation model and an artificially reduced viscosity. This had the effect of dramatically narrowing the shear layers (to the order of the mesh size) and then background flow values were assigned to nodes in the vicinity of the shear layer by extrapolation from the upper or lower domain as appropriate. A system of two potential flow regimes was thus created and is shown in figure 5. No treatment of the non-homentropic or the primary shear layer was attempted

Figure 5: Axial Velocity (Potential Flow)

B.Acoustic Mode Calculations

The wave expansion method was applied as described above with Dirichlet condition $\phi = 1$ at the secondary inlet and $\phi = 0$ on the axis. All the other boundary conditions were hard wall or "radiation" as described above. This included the inlet to the primary jet. In the axisymmetic formulation it will be noted that there are several $\frac{1}{r}$ terms which will become singular close to the axis. In the simulations these terms were ignored once r fell below a threshold with the code showing little sensitivity. The calculations were performed primarily for a no-flow case at the first blade pass frequency at the secondary rotor. The calculations are presented in the case of modes (0,16), (0,20) and (0,22) which can be seen to be non-propagating from figure 7. The high mach number occurring at the exit of the primary jet causes a significant scattering action the effect of which on external propagation would certainly seem to merit further investigation and may be a source of discrepancy between a potential formulation and a full linearised Euler calculation. The shear layer jump was artificially faded out of the range of 3 to 6 diameters from the exit of the secondary jet and is seen to have little effect on the propagation in this case to far field. The calculation runs in a matter of seconds on a modest laptop computer in a matlab environment.

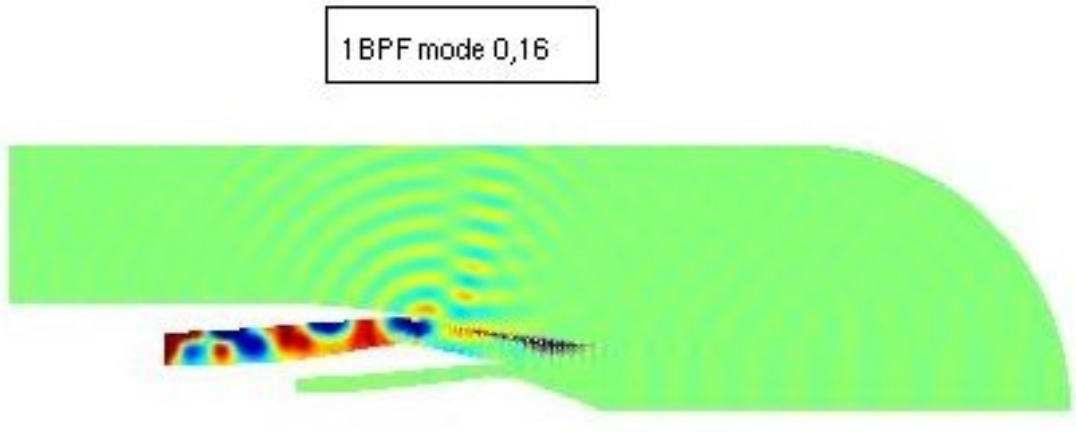

Figure 6: Acoustic potential : mode 16

Figure 7: Acoustic potential : mode 20

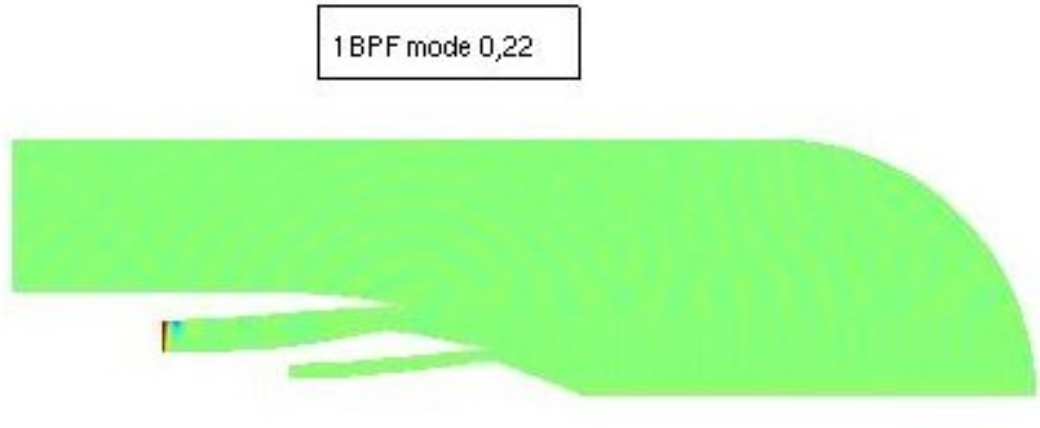

Figure 8: Acoustic potential : mode 22

3.CONCLUSIONS

- The wave based discretisation under a potential flow model generated from a RANS model appears to offer an attractive calculation option for efficient modelling of aft fan noise.
- The natural radiation boundary condition functions very well and allows the use of a single compact mesh over which background flow and acoustical calculations may be performed.
- This finite difference formulation allows the use of standard meshing tools and can directly implement complex boundary and interface conditions.

4.ACKNOWLEDGEMENTS

The authors gratefully acknowledge the support of the EU FP6 NACRE - New Aicraft Concepts REsearch - programme.

References

[1] W. Eversman and D.Okunbar. Aft fan duct acoustic radiation. *Journal of Sound and Vibration*, 213:235–257, 1998.

[2] C. Bailly D.Juve. Numerical solution of acoustic propagation problems using linearized euler equations. *AIAA journal*, 38(1):22–29, 2000.

[3] J.E.Caruthers R.C.Engels G.K.Raviprakash. A wave expansion method for discrete frequency acoustics within inhomogeneous flows. In *AIAA 96-1684, 2nd Joint AIAA/ CEAS Acoustics Conference*, 1996.

[4] G.Gabard. Wave-based discontinuous galerkin methods for the linearized euler equations in the frequency domain. In *13th AIAA/CEAS Conference*, pages 1–8, 2007.

[5] M.S.Howe. *Acoustics of Fluid Structure Interactions*. Cambridge University Press, 1998.

[6] J.E.Caruthers J.C.French G.K.Ravipraksh. Green's function discretization for numerical solution of the helmholtz equation. *Journal of Sound and Vibration*, 187(4):553–568, 1995.

[7] C.Clancy and H.J.Rice. Acoustic Shielding in Low Mach Number Potential Flow Incorporating a Wake Model using BEM. *15th AIAA/CEAS Aeroacoustics Conference*, 2009.